Korean J. Chem. Eng., 34(2), 476-483 (2017)
DOI: 10.1007/s11814-016-0278-0

pISSN: 0256-1115
eISSN: 1975-7220

Fabrication of carbon nanotube-loaded TiO_2@AgI and its excellent performance in visible-light photocatalysis

Liu Yang, Yang An, Bin Dai, Xuhong Guo, Zhiyong Liu, and Banghua Peng†

School of Chemistry and Chemical Engineering, Key Laboratory for Green Process of Chemical Engineering of Xinjiang Bingtuan, Key Laboratory of Materials-Oriented Chemical Engineering of Xinjiang Uygur Autonomous Region, Engineering Research Center of Materials-Oriented Chemical Engineering of Xinjiang Bingtuan, Shihezi University, Shihezi 832003, China

(*Received 2 December 2015 • accepted 11 October 2016*)

Abstract–Novel, visible light driven CNTs-TiO_2@AgI hybrid materials were synthesized by a simple solvothermal-dissolution-precipitation method, during which the acid vapor treated carbon nanotubes (CNTs) as template, AgI as sensitizer and TiO_2 as the bridge unified them to form a ternary composite. The morphology and chemical components of as-prepared samples were characterized by high-resolution transmission electron microscopy (HRTEM), X-ray diffraction (XRD) and X-ray photoelectron spectroscopy (XPS). XRD and XPS characterizations indicated that anatase TiO_2 and crystal AgI co-existed in the composite. HRTEM demonstrated CNTs were decorated with well-dispersed AgI and TiO_2 nanoparticles (NPs), and TiO_2 had an intimate connection with both AgI and CNTs. Diffusive reflectance UV-vis spectroscopy of CNTs-TiO_2@AgI nanocomposite was extended to the whole UV-visible region due to adding of CNTs and AgI NPs. Degradation of Rhodamine B (RhB) polluted water using CNTs-TiO_2@AgI NPs was carried out under visible light irradiation, and it showed higher degradation efficiency than CNTs-TiO_2, TiO_2@AgI, and CNTs@AgI NPs. The primary reason for the enhanced photocatalytic property was attributed to the synergic effect in CNTs-TiO_2@AgI, which included the good adsorption ability and electrical conductivity of CNTs as well as the intimate connection and hetero-junctions among AgI, TiO_2, and CNTs. Meanwhile, the as-prepared hybrid materials can be easily separated and reclaimed from the liquid phase, and the recycling tests indicated CNTs-TiO_2@AgI had renewable performance.

Keywords: Titanium Dioxide, Carbon Nanotubes, Silver Iodide, Photocatalysis

INTRODUCTION

The treatment of industrial waste water to remove organic pollutants is a very important aspect for environmental technology [1-3]. Heterogeneous photocatalysis, as an advanced oxidation technique and a cost-effective means for solar energy utilization and environmental purification, recently has attracted many researchers' attention [4-9]. TiO_2, as a low-cost, non-toxic, stable, highly efficient and environment-friendly semiconductor catalyst, has been extensively used in photocatalytic degradation of organic pollutants [10-12]. Unfortunately, owing to its large band gap, the massive application of TiO_2 has been significantly inhibited for inefficient use of solar energy because TiO_2 responds only to UV light, which accounts for about 5% of the solar spectrum [13]. Fast recombination time for photo-induced electron-hole (e^--h^+) pairs for TiO_2 is also a challenge, which determines the photocatalytic efficiency of TiO_2 [14,15].

Immobilizing TiO_2 on suitable conductive supporting materials had been developed to slow down the fast recombination time for photo-induced e^--h^+ pairs [16-20]. CNTs can be used as an ideal supporter and mediator for TiO_2 to boost its performance in photocatalysis [21-23]. Incorporation of CNTs brings certain potential advantages. First, owing to good electrical conductivity, CNTs can provide effective electron pathways, which may enhance the charge separation by transferring photo-generated electrons, and therefore increase the electron diffusion length and prevent the e^--h^+ recombination [17,24]. Second, the high surface area and one-dimensional morphology of CNTs could serve as a template to regulate the growth of TiO_2 [25-27]; and the surface oxygen functional groups on CNTs act as active sites for the growth of hetero-structure guest materials [28,29], which is very favorable to form an evenly distribution of particles and the hetero-structures are with a good interfacial contact. Homogeneous distribution of nanocrystals on CNTs surface and good interface contact are the essential features for the improved performance [30-32]. Meanwhile, their favorable mechanical strength and chemical stability are vital to keep the physical and chemical properties of catalyst in the photodegradation of organic pollutants. Thus, the CNTs-based structure led to enhanced electronic transport and more hetero-junctions, which is said to extend the recombination time of e^--h^+ pairs [33-35] and result in improved efficiency of photocatalysis [36-38].

TiO_2 optical properties can be tuned by combination or coupling with semiconductor materials, and the development of a visible light responsive photocatalyst based on TiO_2 is vital for its solar energy utilization. Coupling TiO_2 with a visible light sensitizer is a practi-

†To whom correspondence should be addressed.
E-mail: banghuapeng@hotmail.com

cal method to improve its optical properties. Recently, low band gap silver-halide (AgI, AgCl and AgBr) based composites have been used as visible light active photocatalysts [39-41]. Among them, AgI has been considered as a promising visible light photocatalyst because of its smaller band gap than AgBr and AgCl (having band gap of 2.8 eV) [41-44]. Its excellent photocatalytic property has also attracted wide attention, and it has been found that AgI can maintain its stability and enhance the photocatalytic activity when AgI is coupled with TiO_2, CNTs, graphene and g-C_3N_4 [45-47]. Due to the existence of TiO_2 and the conductive substrate, the photo-generated electrons from AgI can be ultimately transferred to O_2 through conduction band of TiO_2, not Ag^+ which led to significantly enhanced stability of AgI, and in this way, the high visible light responsive performance of AgI can be utilized [19,41,44]. Li et al. prepared AgI-TiO_2 nanostructured photocatalyst [48], which displayed high activity for the degradation of 4-chlorophenol under visible light irradiation. Shi et al. prepared a novel plasmonic Ag/AgX-CNTs nanocomposite, which showed high photocatalytic efficiency for the degradation of 2,4,6-tribromophenol [49]. Xu et al. prepared CNTs/AgI through hydrothermal method and proved the enhanced photocatalytic degradation and antibacterial ability [50]. To further increase the photocatalytic activity of CNTs-TiO_2 based photocatalysts, AgI with superior visible light absorption was added to obtain the desired CNTs-TiO_2@AgI nanocomposites. When loading AgI, the hetero-junction structures are formed between AgI and the support materials. It was reported that the hetero-junction structure could significantly increase the photocatalytic activity [51,52]. Therefore, for AgI based composite photocatalysts, construction of composites with appropriate energy band and hetero-junction structure may obtain the high efficiency and stability. If CNTs-TiO_2 loaded AgI hybrid materials are prepared, it is likely that the highly separated CNTs loaded TiO_2-AgI ternary structure with enhanced photocatalytic performance can be obtained. To the best of our knowledge, there have been no reports on the utilization of CNTs-TiO_2 loaded AgI composite photocatalyst system for environmental purification under visible light irradiation.

In this work, visible light driven CNTs-TiO_2@AgI composite photocatalyst was obtained by a two-step conventional solvothermal and facile dissolution-precipitation method. Here, functionalized CNTs were used to act as support material and very good charge transport material, AgI as photoelectron absorber to inspire the catalytic effect, and TiO_2 as the bridge to unify them to form hetero-junction composites. The CNTs-TiO_2@AgI composite exhibited new characteristics and properties that were different from those counterparts. Enhanced photocatalytic activity of CNTs-TiO_2@AgI nanocomposite was assessed by degradation of RhB aqueous solutions under visible light irradiation and compared with that of contrasting samples like CNTs-TiO_2, TiO_2@AgI and CNTs@AgI. The dramatically enhanced degradation efficiency was attributed to the enhanced visible light absorption for CNTs and AgI as excellent sensitizers, fast electron transportation properties for CNTs, which eventually facilitates more efficient separation, easier transferring of photo-generated e^--h^+ pairs to the catalyst surface and more hetero-junction structures to reduce the recombination rate of e^--h^+ pairs. Moreover, recycling tests were performed to investigate the photocatalytic stability and it showed renewable performance of as-prepared catalysts. Finally, a possible degradation mechanism over CNTs-TiO_2@AgI was discussed.

EXPERIMENTAL

1. Materials

CNTs (length 5-15 μm, diameter 10-20 nm, purity >97%) were purchased from Shenzhen Nanotech Port Co., Ltd. Tetrabutyl titanate (TBOT) was purchased from Tianjin Fuchen Chemical Research Institute. Silver nitrate was purchased from Shanghai Shenbo Chemical Co., Ltd. Polyvinylpyrrolidone (PVP) K-40 (Mw≈40000) was purchased from Amresco. Nitric acid and Potassium iodide were purchased from Chengdu Kelong Chemical Plant. Absolute ethanol, ethylene glycol (EG) and acetic acid were produced by Tianjin Chemical Reagent Factory. RhB was purchased from Tianjin Guangfu Fine Chemical Research Institute. All the chemicals were used without further purification.

2. Preparation of CNTs-TiO_2

Modification of CNTs was by acid vapor treating method as described in our previous paper [53,54]. The purification step introduced oxygenated functionalities onto CNTs surface, which can nucleate NPs and also prevent NPs from agglomeration [55]. CNTs-TiO_2 were prepared through solvothermal method. Typically, 4.5 mL of TBOT was dissolved in 20 mL ethanol under magnetic stirring for 10 min to constitute solution A. 50 mg modified CNTs were dispersed in another 20 mL ethanol with ultrasonication for 10 min, and then 2 mL of acetic acid was added into CNTs-ethanol solution, with nitric acid regulating the pH about 2-3 to prepare solution B. After that, solution A was slowly dropped into the solution B under stirring for 15 min. The resulting suspension was stirred for 1 h in water bath at 60 °C. Subsequently, it was transferred into a 100 ml Teflon-lined, stainless autoclave and stored in oven at 180 °C for 6 h. Finally, the products were separated by filtration or centrifugation and washed carefully with ethanol to remove organic species. Filtrates were dried in oven at 60 °C for 12 h to obtain the CNTs-TiO_2 nanocomposite.

Because of the oxygenated functionalized CNTs, TiO_2 particles will nucleate on CNTs surface. From the stock additive amount, the 5% weight percentage of CNTs in TiO_2-CNTs can be deduced, but gray dark precipitates were produced.

3. Synthesis of CNTs-TiO_2@AgI Nanocomposite

AgI attached CNTs-TiO_2 were prepared as n the following procedure. The aforementioned CNTs-TiO_2 0.05 g was dispersed into 60 mL of EG, and the suspension was under ultrasonic agitation for 10 min. 0.05 g PVP and 0.06 g silver nitrate were successively added into the suspension under magnetically stirring for 30 min until they were completely dissolved. Then a 10 mL EG solution of potassium iodide (0.08 g) was slowly added and the resulting mixture solution was heated at 60 °C for 1 h. The obtained product was separated and rinsed for several times with deionized water and absolute ethanol, respectively. Finally, the yellowish dark precipitation was dried at 60 °C for 12 h in vacuum oven. The calculated weight percentage for AgI in hybrid was kept at ~62%. Scheme 1 gives the preparation illustration for CNTs-TiO_2@AgI nanocomposite.

4. Synthesis of CNTs @AgI and TiO_2 @AgI Nanocomposites

The contrast sample AgI attached CNTs (CNTs@AgI) was pre-

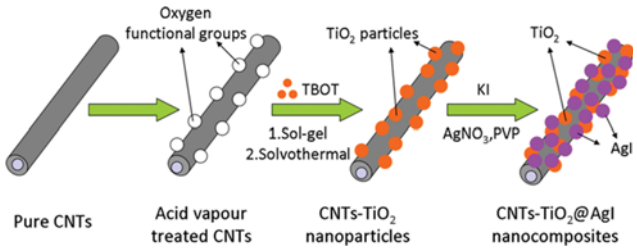

Scheme 1. Schematic for preparation of CNTs-TiO_2@AgI nanocomposite.

pared by using a similar method. 50 mg CNTs, instead of CNTs-TiO_2 was added in 60 mL EG and the following steps were kept the same as the preparation of CNTs-TiO_2@AgI.

For synthesis of TiO_2 loaded AgI (TiO_2@AgI), firstly, 4.5 mL of TBOT was dissolved in 20 mL ethanol under magnetic stirring for 10 min, and then 2 mL of acetic acid was added into it, with nitric acid regulating the pH about 2-3. The resulting suspension was stirred for 1 h in water bath at 60 °C. Subsequently, it was transferred into a 50 ml Teflon-lined stainless autoclave, stored in oven at 180 °C for 6 h. TiO_2 powders were obtained by filtration and drying in oven at 60 °C for 12 h. Secondly, AgI was loaded on synthesized TiO_2, and the procedures were the same as that for TiO_2-CNTs@AgI, except the addition of 50 mg TiO_2.

5. Evaluation of Photocatalytic Performance

Photocatalytic activity of as-synthesized samples was evaluated by photodegradation of RhB solution under visible light irradiation. In a typical procedure, 10 mg of as-prepared catalysts was dispersed into a 20 mL RhB aqueous solution with the concentration of 5 mg L^{-1} in a 100 mL quartz beaker. Prior to irradiation, the suspensions were magnetically stirred in the dark for 1 h to establish adsorption/desorption equilibrium between RhB and the surface of catalyst under room conditions. 300 W Xenon arc lamp (CEL-HXF300) equipped with a 420 nm UV cut-off filter about 10 cm away from the reactant solution was used as the visible light source for photodegradation. The intensity of light source was 200 mW cm^{-2}.

At given irradiation time intervals, aliquots of solution were collected and centrifuged to remove the particles, and the top solution was transferred to a cuvette for UV-vis measurement. Contrast experiments with CNTs-TiO_2, CNTs@AgI, TiO_2@AgI as the photocatalysts were also carried out under identical conditions. Degradation efficiency was calculated based on the following equation: RhB degradation efficiency (%)=$(A_0-A)/A_0\times100\%$ (it was thought that the concentration ratio C/C_0 is equal to the ratio of absorbance A/A_0). Here, A is the absorption of RhB solution at each irradiated time interval for the main peak in the adsorption spectrum, and A_0 is the absorption of initial concentration C_0 when the adsorption-desorption equilibrium is reached.

When recycle stability experiments were carried out, all the precipitates were collected through centrifugation, and dried in oven at 60 °C, which were re-used in the consecutive test.

RESULTS AND DISCUSSION

1. Structure, Morphology and Crystallinity Analysis

The typical surface structure and morphology of prepared composites was investigated by HRTEM (Tecnai G2 F20, FEI). For sample preparation, a small amount of solid powder was added in absolute ethanol by ultrasonic dispersion for 15 minutes. Then, a small part of the suspending liquid was dropped onto copper meshes to do test. The TEM images of pure CNTs, CNTs-TiO_2, and CNTs-TiO_2@AgI nanocomposite were represented in Fig. 1. The pristine CNTs with diameters 10-20 nm can be clearly seen as the hollow tubes form in Fig. 1(a), which agreed well with the size of purchased product. Image of CNTs-TiO_2 is shown in Fig. 1(b). It seemed the TiO_2 NPs were dispersed evenly on the surface of CNTs, and the size was less than 10 nm. Fig. 1(c) shows the structure of CNTs-TiO_2@AgI, and a few black dots can be observed in this image. Owing to AgI and TiO_2 both being small particles, they cannot be distinguished easily, except the particles with the shades of color, showing the black particles were AgI NPs and the gray particles were TiO_2 [56,57]. The average size of these particles was in nanoscale range, and they were compact, uniform with no abnormality, which can be attributed to the inductive effect of CNTs in the composite. The AgI and TiO_2 nanocrystals anchoring on the surface of CNTs looked like a rivet and had a good dispersion behavior on the surface, which could offer more hetero-junction and photocatalytic reaction centers. Therefore, it was expected to offer an increased photocatalytic activity.

To further obtain the composition information of CNTs-TiO_2@AgI

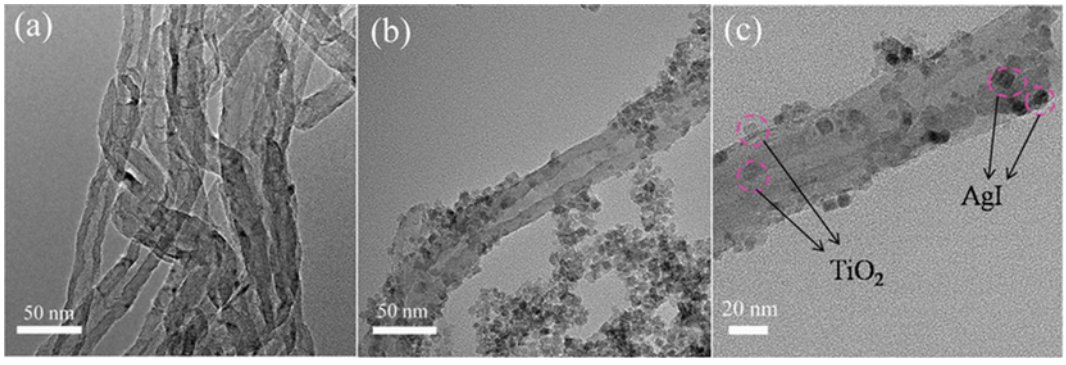

Fig. 1. HRTEM images of pristine CNTs (a); CNTs-TiO_2 (b) and CNTs-TiO_2@AgI nanocomposite (c). The circles in (c) indicates TiO_2 or AgI NPs.

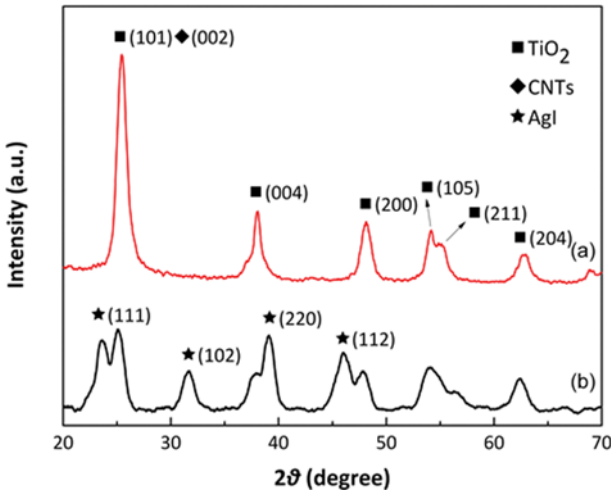

Fig. 2. XRD patterns of (a) CNTs-TiO_2 and (b) CNTs-TiO_2@AgI nanocomposite.

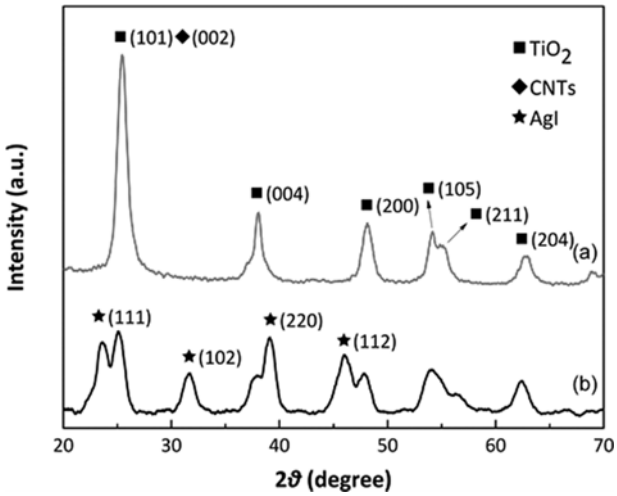

Fig. 3. XPS spectrum of CNTs-TiO_2@AgI nanocomposite.

and the crystallinity of the nanocomposite, X-ray diffraction (XRD, Bruker D8 Advance) was characterized using Cu Kα (λ=0.154056 nm) radiation under 40 KV and 40 mA condition, scanning over the range of $20^{\circ} \leq 2\theta \leq 70^{\circ}$. The XRD patterns of CNTs-TiO_2 and CNTs-TiO_2@AgI nanocomposite are given in Fig. 2. It observed that some sharp diffraction peaks appeared from the pattern of the CNTs-TiO_2 at 2θ value ca. 25°, 36°, 47°, 54° and 62°, which corresponded to the (101), (004), (200), (105), and (204) crystal planes of anatase TiO_2 (JCPDS No. 21-1272). Notably, diffraction peaks for CNTs failed to be observed in XRD of the CNTs-TiO_2 nanocomposite, which might be due to the overlap of the intense peak of anatase TiO_2 (101) reflection with that of the CNTs (002), together with the low amount and low diffraction intensity of CNTs in the nanocomposite [53,58,59]. Compared with CNTs-TiO_2 nanocomposite, CNTs-TiO_2@AgI nanocomposite showed some new peaks at 2θ value ca. 23°, 32°, 39° and 46°, which are attributed to the (111), (102), (220), and (112) crystal planes of AgI (JCPDS No. 09-0399). No impurity phase was detected. The broadening of these diffraction peaks indicated that the sample was nano-sized, and the crystalline size of the sample was estimated to be 10 nm from the Scherrer equation [60]. Thus, the XRD results demonstrated that AgI and TiO_2 NPs were successfully synthesized, and this conclusion accorded well with TEM results.

X-ray photoelectron spectroscopy (XPS, AMICUS ESCA3400) analysis was further employed to determine the chemical composition and bonding configuration of as-fabricated products, and the results are shown in Fig. 3. It shows the characteristic energy peaks of element Ti, O, C, Ag and I, with binding energy E_b=464.1 eV (Ti 2p), E_b=529.75 eV (O 1s), E_b=284.6 eV (C 1s), E_b=367.2 eV (Ag 3d) and E_b=618.8 eV (I 3d). The binding energy of Ag $3d_{5/2}$ (367.2 eV) was assigned to Ag^+ of AgI, which means that Ag species exists in the form of AgI without detectable Ag^0 species [61]. The XPS peak of I $3d_{5/2}$ appears at 618.8 eV, which is also assigned to I^- in AgI [58]. No impurity elements existed, and all these results indicated CNTs-TiO_2@AgI nanocomposite with high purity had been successfully synthesized in this study.

2. Absorption Properties, Photocatalysis and Stability Performance

There is a great need for structuring photocatalyst related to band gap (E_g) and size to optimize the absorption properties. UV-

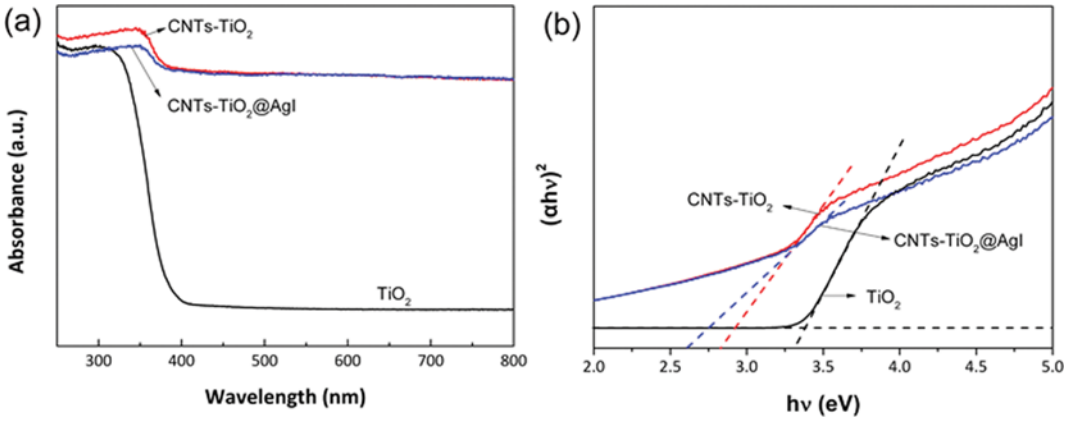

Fig. 4. (a) Wavelength-dependent absorbance and (b) Kubelka-Munk transformed reflectance spectra of TiO_2, CNTs-TiO_2 and CNTs-TiO_2@AgI nanocomposite.

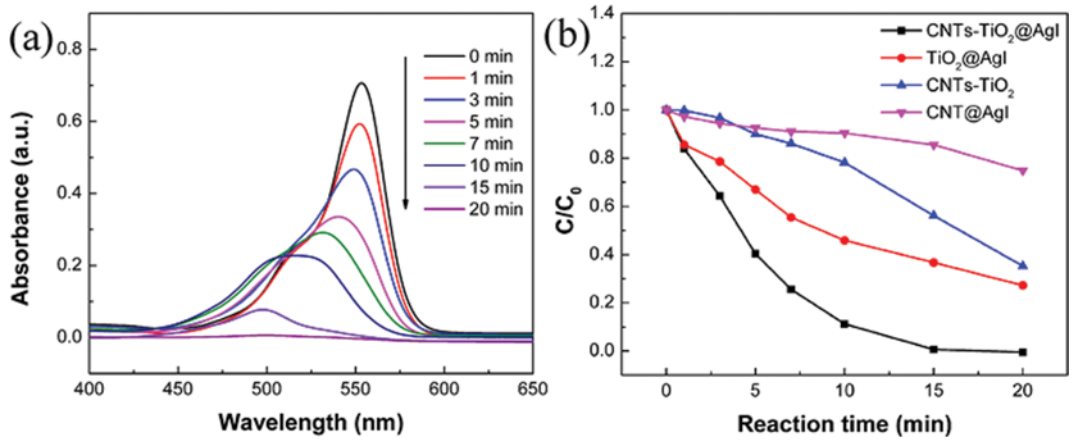

Fig. 5. (a) UV-vis spectra of RhB solution under different irradiation time using CNTs-TiO_2@AgI; (b) comparison of degradation efficiency for CNTs-TiO_2@AgI, CNTs-TiO_2, CNTs@AgI and TiO_2@AgI.

vis absorption spectrum can be used to evaluate E_g of semiconductors. Here, UV-vis diffuse reflectance spectra (Tu-1901, Beijing Persee) were measured using $BaSO_4$ as the reference, displayed in Fig. 4(a), and the measurements were converted to absorbance spectra using the Kubelka-Munk method [62]. For TiO_2, absorption edge around 370 nm corresponds to its E_g of 3.36 eV, and no visible light absorption in the range of 400 nm to 800 nm was observed. It is clearly seen from the plot that CNTs-TiO_2 powders and CNTs-TiO_2@AgI composite exhibited stronger visible light absorption when compared with pure TiO_2, and even covered the whole range of measured UV-vis region, which was in accordance with the color changing from white to dark. This enhanced absorption could be attributed to the presence of CNTs and AgI, which were sensitizers and increased visible light absorption [58,61]. Another reason is the even distribution of TiO_2 and AgI NPs on CNTs. The unpaired π electrons in CNTs may cause the interaction with TiO_2 and AgI NPs; such interaction might shift the band edge and increase the light absorption towards the visible region [56,63]. The CNTs-TiO_2 sample showed stronger broad absorption and had higher intensity in the UV range compared with the CNTs-TiO_2@AgI, which was unified with the color changing from gray black to yellowish black.

The E_g of photocatalysts can be calculated using the following formula: $\alpha = A(hv - E_g)^{1/2}/hv$, where a is the absorption coefficient, A is proportional constant, h is the Planck's constant, v is the frequency of incident light [44,62]. The corresponding Kubelka-Munk transformed reflectance spectra are shown as the curve in Fig. 4(b) where the slopes of the tangents on horizontal axis are E_g energies. The calculated E_g for TiO_2 is 3.4 eV (corresponding to the absorption edge 400 nm), consistent with the anatase phase TiO_2, while the narrower E_g approximately 2.6 eV (corresponding to the absorption edge of 450 nm) for CNTs-TiO_2@AgI photocatalysis is very suitable for visible light response. At the same time, CNTs-TiO_2@AgI affords a smaller E_g than that of 2.8 eV for CNTs-TiO_2, showing that CNTs-TiO_2@AgI should have more electrons to be excited than CNTs-TiO_2 when irradiated, and this speculation can be identified by the degradation experiments.

To verify the improved photocatalytic activity of CNTs-TiO_2@AgI nanocomposite, we investigated the experiments for degradation RhB solution, which is a well-known organic dye pollutant in wastewater produced from textile and other industrial processes. The photo-degradation results shown in Fig. 5(a) clearly indicate that a characteristic absorption peak of RhB molecules located at ~554 nm was weakened gradually with increasing visible light exposure and almost fully degraded after irradiation for 20 min, which implied the CNTs-TiO_2@AgI nanocomposite was effective photocatalyst for degradation of RhB solution. Fig. 5(b) shows the changes in relative concentration (C/C_0) of RhB solution versus time containing CNTs-TiO_2@AgI, CNTs-TiO_2, CNTs@AgI and TiO_2@AgI nanocomposite under identical visible light irradiation. It is clearly demonstrated that CNTs-TiO_2@AgI nanocomposite showed best performance within these four composite catalysts, because its degradation rate in C/C_0 was faster under the same time, and the degradation efficiency for CNTs-TiO_2@AgI nanocomposite reached 100.0% after being exposed to visible light for 15 min, which was higher than that of TiO_2@AgI (63.3%), CNTs-TiO_2 (43.9%), and CNTs@AgI (14.5%). This conclusion was also confirmed by the absorption and E_g analysis (see the Absorption analysis).

The importance of CNTs addition is evident when comparing the degradation results for CNTs-TiO_2@AgI and TiO_2@AgI, which is due to the intense visible light absorption for CNTs and the conductive property that is advantageous for NPs loading, electron transferring and storage [31].

When comparing degradation between CNTs-TiO_2@AgI and CNTs@AgI, we found that the photocatalytic effect for CNTs@AgI was inferior to that of CNTs-TiO_2@AgI, and even it was worst among these materials. It could be explained by TiO_2 bridging effect among AgI and CNTs, which makes hetero-junctions between them (see Fig. 1 and TEM analysis). The hetero-junction in CNTs-TiO_2@AgI might be the key factor to the enhanced performance [19]. If we compare TiO_2@AgI with CNTs@AgI (the AgI loading is the same) for the photocatalytic results, it is evident that they showed different performance, which corroborated that the TiO_2-AgI hetero-junction was much more crucial to the degradation effect than that between CNTs and AgI. The detailed discussion is presented in the mechanism discussion section.

The effect of AgI is obvious when contrasting the curves for CNTs-TiO_2@AgI and CNTs-TiO_2 in Fig. 5(b). Without AgI, the performance was not so good even though their absorptions showed the same trend in the visible region (see Fig. 4(a)). The E_g for CNTs-TiO_2@AgI was smaller than that of CNTs-TiO_2, and also more hetero-junctions existed in CNTs-TiO_2@AgI than in CNTs-TiO_2, which again indicated the importance of AgI sensitization and the hetero-junction effect, especially the TiO_2-AgI hetero-junction.

For the other contrast, such as TiO_2@AgI with CNTs-TiO_2, we can get that photocatalytic effect of TiO_2@AgI was better than that of CNTs-TiO_2, mainly highlighting the AgI sensitization performance. Note that the weight percentage for AgI in TiO_2@AgI hybrid is extremely higher than that of CNTs in CNTs-TiO_2 (see the explanation in Preparation Section); maybe this is another reason for the better performance for TiO_2@AgI.

Besides photocatalytic activity, the stability of photocatalysts is also very important for practical application. To compare the stability of the as-prepared photocatalysts, we conducted five repeatability experiments of RhB dyes degradation over CNTs-TiO_2@AgI, and the results are shown in Fig. 6. The degradation efficiencies did not exhibit any significant loss after five runs of degradation, which indicated that CNTs-TiO_2@AgI had high stability and could not be photo-corroded during the photocatalytic oxidation of RhB molecules. In addition, the re-used CNTs-TiO_2@AgI showed the same color as the newly prepared catalyst. Thus, CNTs-TiO_2@AgI composite is promising for practical applications in environmental purification, and our work also suggests that by exploring more physical and chemical properties, the CNTs-TiO_2@AgI system can be used as an efficient catalytic material.

3. The Mechanism of Photoactivity Enhancement

The photocatalytic activity of catalysts depends on many factors, such as crystallinity, morphology and optical property [20,64-66]. For the first influence factor, crystallinity can be excluded because main components of our samples do not change their crystal form (See Fig. 2, XRD analysis). Here, our research is focused on the combination effect of various components, and not on the changes of crystallinity. Many studies confirm that the size effect of materials could be considered as an important factor to increase the photocatalytic activity [56]. Second, optical property is an also important factor for high activity of hybrid materials. The CNTs-TiO_2@AgI hybrid showed an intense, broad background absorption in the visible light region (as shown in Fig. 4(a)), and the E_g for it was smaller than TiO_2-CNTs. This result indicated that the hybrid could absorb more photons, which was favorable for the degradation reaction. Third, the high photocatalytic behavior of our CNTs-TiO_2@AgI hybrid materials might also be assigned to a better dispersion and a small size of AgI and TiO_2 on the CNTs surface compared with their counterparts (see Fig. 1, TEM analysis), which was proved by the degradation results. Finally, the electron transfer at the hetero-junction interfaces should also affect photocatalytic performance [52]. When the AgI NPs were introduced to CNTs-TiO_2, two types of semiconductor materials combined closely and there formed two hetero-junction structures with CNTs, which could efficiently separate the e^--h^+ pairs in the two materials that cause enhanced photo-performance.

According to the above analysis, a tentative mechanism is proposed for the high photocatalytic activity of our hetero-structure. Scheme 2 illustrates the possible photocatalytic mechanisms involved in the activation of photocatalytic reaction by CNTs-TiO_2@AgI nanocomposite. First, the high specific surface area of CNTs is beneficial to accept the large quantities evenly distributed of AgI and TiO_2 NPs, which is beneficial to electron transfer and storage. CNTs also increase the absorption intensity, expanding the light absorption range. When AgI was added, the light absorption range was further enlarged, which is favorable for light absorption of photocatalysts. Second, under visible light irradiation, narrow band gap semiconductor AgI are easier to be sensitized than CNTs-TiO_2, absorbing the visible light and the valence band electrons are excited to the conduction band, and then they are immediately transferred to the conduction band of TiO_2 through the intimate contacts especially at the TiO_2-AgI interface. Simultaneously, CNTs are good electron acceptors and can also accept the excited electrons from the AgI particles, too, which supplies another electron transfer channel. This mechanism implied that there were three reaction sites in

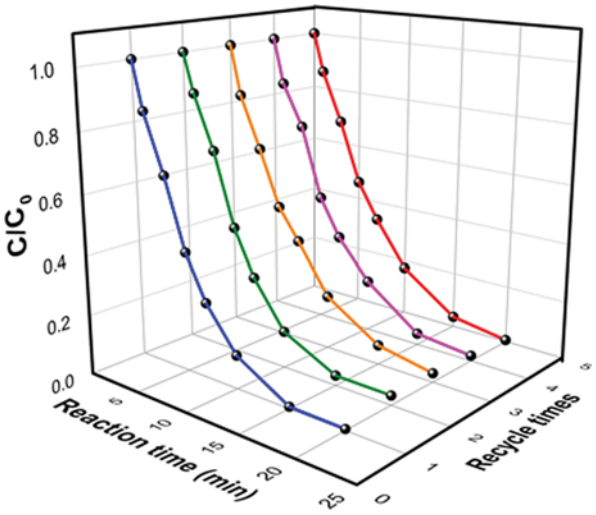

Fig. 6. Cyclic test for CNTs-TiO_2@AgI nanocomposites under visible light irradiation.

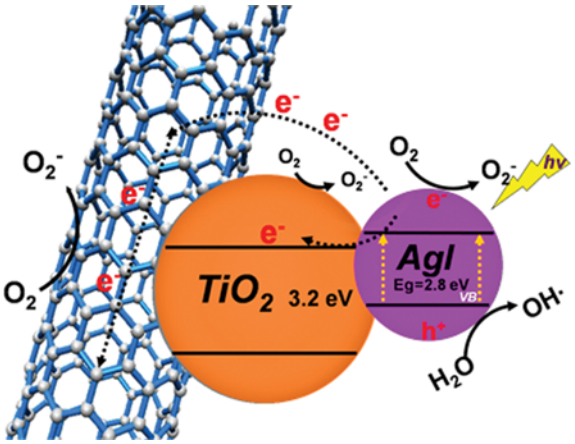

Scheme 2. Schematic illustration of charge transfer process in CNTs-TiO_2@AgI nanocomposite under visible light irradiation.

CNTs-TiO_2@AgI nanocomposite (Scheme 2) that are the interfaces of CNTs, TiO_2 and AgI, and it is this configuration that determined the photocatalytic efficiency. Finally, the hetero-junction structures cannot be neglected in our samples. These junctions can efficiently separate the e^--h^+ pairs; thus the produced e^--h^+ pairs recombination is decreased and more time is available for producing more reactive oxygen species such as •OH and $•O_2^-$ with especially oxidation capability to enhance the photocatalytic activity [34]. In short, the unique hetero-structure of CNTs-TiO_2@AgI results in the high photocatalytic degradation efficiency.

CONCLUSION

We have introduced a simple solvothermal method to prepare CNTs-TiO_2, and through dissolution-precipitation doping AgI on the surface to obtain CNTs-TiO_2@AgI nanocomposite. Based on the TEM and XRD characterization, nanometer-sized crystalline anatase TiO_2 and AgI NPs were successfully anchored on CNTs. The results of photodegradation RhB experiments demonstrated that CNTs-TiO_2@AgI nanocomposite exhibited a significant increment of photocatalytic activity in comparison to the CNTs-TiO_2, TiO_2@AgI, and CNTs@AgI counterparts. The enhanced photocatalytic activity of CNTs-TiO_2@AgI nanocomposite is attributed to CNTs and AgI as excellent sensitizer to modify TiO_2 to be visible light responsive, and the capability of CNTs as a template to regulate the growth of TiO_2 and AgI, acting as good electron acceptors to facilitate the separation of photo-generated e^--h^+ pairs at the hetero-junctions of CNTs-TiO_2@AgI nanocomposite. The synthesis route and materials properties demonstrated in this paper will open up new opportunities for fabrication of photocatalysis materials for environmental applications.

ACKNOWLEDGEMENTS

This work was supported by National Natural Science Foundation of China (21663023), Bingtuan Innovation Team in Key Areas (2015BD003) and Open Project for Key Laboratory of Materials-Oriented Chemical Engineering of Xinjiang Uygur Autonomous Region (2015BTRC004).

REFERENCES

1. A. Fujishima, X. T. Zhang and D. A. Tryk, *Surf. Sci. Rep.*, **63**, 515 (2008).
2. A. Di Paola, E. Garcia-Lopez, G. Marci and L. Palmisano, *J. Hazard. Mater.*, **211**, 3 (2012).
3. M. Ahmadi, P. Amiri and N. Amiri, *Korean J. Chem. Eng.*, **32**, 1327 (2015).
4. H. Zhang, X. Fan, X. Quan, S. Chen and H. Yu, *Environ. Sci. Technol.*, **45**, 5731 (2011).
5. M. Guan, C. Xiao, J. Zhang, S. Fan, R. An, Q. Cheng, J. Xie, M. Zhou, B. Ye and Y. Xie, *J. Am. Chem. Soc.*, **135**, 10411 (2013).
6. Z. Xiong and X. S. Zhao, *J. Am. Chem. Soc.*, **134**, 5754 (2012).
7. C. Karunakaran, S. Kalaivani and P. Vinayagamoorthy, *Mater. Lett.*, **122**, 21 (2014).
8. D. Tsukamoto, Y. Shiraishi, Y. Sugano, S. Ichikawa, S. Tanaka and T. Hirai, *J. Am. Chem. Soc.*, **134**, 6309 (2012).
9. H. M. Yadav, J. S. Kim and S. H. Pawar, *Korean J. Chem. Eng.*, **33**, 1989 (2016).
10. M. R. Hoffmann, S. T. Martin, W. Choi and D. W. Bahnemann, *Chem. Rev.*, **95**, 69 (1995).
11. A. Fujishima and K. Honda, *Nature*, **238**, 37 (1972).
12. Q. Wang, X. D. Shi, E. Q. Liu, J. J. Xu, J. C. Crittenden, Y. Zhang and Y. Q. Cong, *Ind. Eng. Chem. Res.*, **55**, 4897 (2016).
13. C. An, W. Jiang, J. Wang, S. Wang, Z. Ma and Y. Li, *Dalton Transactions*, **42**, 8796 (2013).
14. X. B. Chen and C. Burda, *J. Am. Chem. Soc.*, **130**, 5018 (2008).
15. Y. F. Ma, J. L. Zhang, B. Z. Tian, F. Chen and L. Z. Wang, *J. Hazard. Mater.*, **182**, 386 (2010).
16. W. Q. Fan, Q. H. Lai, Q. H. Zhang and Y. Wang, *J. Phys. Chem. C*, **115**, 10694 (2011).
17. Y. Yao, G. Li, S. Ciston, R. M. Lueptow and K. A. Gray, *Environ. Sci. Technol.*, **42**, 4952 (2008).
18. S. Kim and S. K. Lim, *Appl. Catal. B-Environ.*, **84**, 16 (2008).
19. D. D. Yu, J. Bai, H. O. Liang, T. F. Ma and C. P. Li, *J. Mol. Catal. a-Chem.*, **420**, 1 (2016).
20. K. Ullah, A. Ullah, A. Aldalbahi, J. D. Chung and W. C. Oh, *J. Mol. Catal. a-Chem.*, **410**, 242 (2015).
21. C. Y. Yen, Y. F. Lin, C. H. Hung, Y. H. Tseng, C. C. Ma, M. C. Chang and H. Shao, *Nanotechnology*, **19**, 219 (2008).
22. J. G. Yu, T. T. Ma and S. W. Liu, *Phys. Chem. Chem. Phys.*, **13**, 3491 (2011).
23. S. Muduli, W. Lee, V. Dhas, S. Mujawar, M. Dubey, K. Vijayamohanan, S. H. Han and S. Ogale, *Acs Appl. Mater. Inter.*, **1**, 2030 (2009).
24. A. Kongkanand, R. M. Dominguez and P. V. Kamat, *Nano Lett.*, **7**, 676 (2007).
25. W. J. Lee, J. M. Lee, S. T. Kochuveedu, T. H. Han, H. Y. Jeong, M. Park, J. M. Yun, J. Kwon, K. No, D. H. Kim and S. O. Kim, *Acs Nano*, **6**, 935 (2012).
26. C. Y. Hsu, D. H. Lien, S. Y. Lu, C. Y. Chen, C. F. Kang, Y. L. Chueh, W. K. Hsu and J. H. He, *Acs Nano*, **6**, 6687 (2012).
27. M. Cargnello, M. Grzelczak, B. Rodriguez-Gonzalez, Z. Syrgiannis, K. Bakhmutsky, V. La Parola, L. M. Liz-Marzan, R. J. Gorte, M. Prato and P. Fornasiero, *J. Am. Chem. Soc.*, **134**, 11760 (2012).
28. X. W. Wang, L. C. Yin and G. Liu, *Chem. Commun.*, **50**, 3460 (2014).
29. H. L. Wang, J. T. Robinson, G. Diankov and H. J. Dai, *J. Am. Chem. Soc.*, **132**, 3270 (2010).
30. Q. J. Xiang, J. G. Yu and M. Jaroniec, *Chem. Soc. Rev.*, **41**, 782 (2012).
31. L. H. Huang, H. J. Wang, Y. L. Liu, Z. B. Jiao and Z. B. Shao, *Prog. Chem.*, **22**, 867 (2010).
32. H. Zhang, X. J. Lv, Y. M. Li, Y. Wang and J. H. Li, *Acs Nano*, **4**, 380 (2010).
33. G. Liu, J. C. Yu, G. Q. Lu and H. M. Cheng, *Chem. Commun.*, **47**, 6763 (2011).
34. K. Woan, G. Pyrgiotakis and W. Sigmund, *Adv. Mater.*, **21**, 2233 (2009).
35. K. F. Zhou, Y. H. Zhu, X. L. Yang, X. Jiang and C. Z. Li, *New J. Chem.*, **35**, 353 (2011).
36. A. I. Hochbaum and P. D. Yang, *Chem. Rev.*, **110**, 527 (2010).
37. A. G. Hu, S. Liu and W. B. Lin, *Rsc. Adv.*, **2**, 2576 (2012).
38. S. Hoang, S. P. Berglund, N. T. Hahn, A. J. Bard and C. B. Mullins,

J. Am. Chem. Soc., **134**, 3659 (2012).
39. H. Wang, J. Gao, T. Q. Guo, R. M. Wang, L. Guo, Y. Liu and J. H. Li, *Chem. Commun.*, **48**, 275 (2012).
40. M. Abou Asi, C. He, M. H. Su, D. H. Xia, L. Lin, H. Q. Deng, Y. Xiong, R. L. Qiu and X. Z. Li, *Catal. Today*, **175**, 256 (2011).
41. R. Vinoth, P. Karthik, C. Muthamizhchelvan, B. Neppolian and M. Ashokkumar, *Phys. Chem. Chem. Phys.*, **18**, 5179 (2016).
42. H. S. Liu, Y. H. Wang, C. C. Li and C. Y. Tai, *Chem. Eng. J.*, **183**, 466 (2012).
43. R. Makiura, T. Yonemura, T. Yamada, M. Yamauchi, R. Ikeda, H. Kitagawa, K. Kato and M. Takata, *Nat. Mater.*, **8**, 476 (2009).
44. Q. Wang, X. D. Shi, J. J. Xu, J. C. Crittenden, E. Q. Liu, Y. Zhang and Y. Q. Cong, *J. Hazard. Mater.*, **307**, 213 (2016).
45. Y. Z. Li, H. Zhang, Z. M. Guo, J. J. Han, X. J. Zhao, Q. N. Zhao and S. J. Kim, *Langmuir*, **24**, 8351 (2008).
46. C. Hu, X. X. Hu, L. S. Wang, J. H. Qu and A. M. Wang, *Environ. Sci. Technol.*, **40**, 7903 (2006).
47. D. Y. Wu and M. C. Long, *Surf. Coat. Tech.*, **206**, 1175 (2011).
48. Y. Li, H. Zhang, Z. Guo, J. Han, X. Zhao, Q. Zhao and S.-J. Kim, *Langmuir*, **24**, 8351 (2008).
49. H. Shi, J. Chen, G. Li, X. Nie, H. Zhao, P.-K. Wong and T. An, *ACS Appl. Mater. Interf.*, **5**, 6959 (2013).
50. Y. G. Xu, S. Q. Huang, H. Y. Ji, L. Q. Jing, M. Q. He, H. Xu, Q. Zhang and H. M. Li, *Rsc. Adv.*, **6**, 6905 (2016).
51. L. X. Yang, S. L. Luo, Y. Li, Y. Xiao, Q. Kang and Q. Y. Cai, *Environ. Sci. Technol.*, **44**, 7641 (2010).
52. J. Jiang, X. Zhang, P. B. Sun and L. Z. Zhang, *J. Phys. Chem. C*, **115**, 20555 (2011).
53. Y. An, J. Hou, Z. Y. Liu and B. H. Peng, *Mater. Chem. Phys.*, **148**, 387 (2014).
54. J. Ming, Y. Q. Wu, Y. C. Yu and F. Y. Zhao, *Chem. Commun.*, **47**, 5223 (2011).
55. T. W. Ebbesen, P. M. Ajayan, H. Hiura and K. Tanigaki, *Nature*, **367**, 519 (1994).
56. H. Xu, J. Yan, Y. G. Xu, Y. H. Song, H. M. Li, J. X. Xia, C. J. Huang and H. L. Wan, *Appl. Catal. B-Environ.*, **129**, 182 (2013).
57. W. Sun, Y. Z. Li, W. Q. Shi, X. J. Zhao and P. F. Fang, *J. Mater. Chem.*, **21**, 9263 (2011).
58. L. Cai, T. Xu, J. Y. Shen and W. X. Xiang, *Mat. Sci. Semicon. Proc.*, **37**, 19 (2015).
59. Y. An, L. Yang, J. Hou, Z. Y. Liu and B. H. Peng, *Opt. Mater.*, **36**, 1390 (2014).
60. D. A. Reddy, J. Choi, S. Lee, R. Ma and T. K. Kim, *Rsc. Adv.*, **5**, 67394 (2015).
61. H. X. Shi, J. Y. Chen, G. Y. Li, X. Nie, H. J. Zhao, P. K. Wong and T. C. An, *Acs Appl. Mater. Inter.*, **5**, 6959 (2013).
62. J. H. Yi, L. L. Huang, H. J. Wang, H. Yu and F. Peng, *J. Hazard. Mater.*, **284**, 207 (2015).
63. J. X. Liu, Y. L. Luan, C. H. An, J. Zhang, D. S. Wang and Y. D. Li, *Chemcatchem*, **7**, 2918 (2015).
64. J. B. Joo, Q. Zhang, M. Dahl, I. Lee, J. Goebl, F. Zaera and Y. D. Yin, *Energy Environ. Sci.*, **5**, 6321 (2012).
65. H. Y. Liu, J. B. Joo, M. Dahl, L. S. Fu, Z. Z. Zeng and Y. D. Yin, *Energy Environ. Sci.*, **8**, 286 (2015).
66. Z. H. Fan, F. M. Meng, M. Zhang, Z. Y. Wu, Z. Q. Sun and A. X. Li, *Appl. Surf. Sci.*, **360**, 298 (2016).